Numerical Optimization Studies of Cardiovascular–Rotary Blood Pump Interaction

*Einly Lim, †Socrates Dokos, ‡Robert F. Salamonsen, ‡Franklin L. Rosenfeldt,
†Peter J. Ayre, and †Nigel H. Lovell

*Department of Biomedical Engineering, Faculty of Engineering, University of Malaya, Kuala Lumpur, Malaysia;
†Graduate School of Biomedical Engineering, University of New South Wales, Sydney, Australia; and ‡Department of
Surgery, Alfred Hospital, Melbourne, Australia

Abstract: A heart–pump interaction model has been developed based on animal experimental measurements obtained with a rotary blood pump in situ. Five canine experiments were performed to investigate the interaction between the cardiovascular system and the implantable rotary blood pump over a wide range of operating conditions, including variations in cardiac contractility and heart rate, systemic vascular resistance (SVR), and total blood volume (V_{total}). It was observed in our experiments that SVR decreased with increasing mean pump speed under the healthy condition, but was relatively constant during the speed ramp study under reduced cardiac contractility conditions. Furthermore, we also found a significant increase in pulmonary vascular resistance with increasing mean pump speed and decreasing total blood volume, despite a relatively constant SVR. Least squares parameter estimation methods were utilized to fit a subset of model parameters in order to achieve better agreement with the experimental data and to evaluate the robustness and validity of the model under various operating conditions. The fitted model produced reasonable agreement with the experimental measurements, both in terms of mean values and steady-state waveforms. In addition, all the optimized parameters were within physiological limits. **Key Words:** Heart–pump interaction model—Implantable rotary blood pump—Heart failure—Ventricular assist devices.

With the advancement of implantable rotary blood pump (IRBP) technology, as well as evidences demonstrating successful outcomes for prolonged periods of implantation (1), IRBPs have moved from bridge-to-transplant to bridge-to-recovery or permanent support for chronic heart failure patients. In order to maximize the quality of life of the implant recipients so that they could regain a normal lifestyle in a long-term unsupervised environment, it is believed that a physiologically responsive pump control strategy which automatically adjusts the pump speed to cater for changes in metabolic demand is needed. If pump control is not properly implemented, underpumping or overpumping may occur when there is a change in

the circulatory conditions, for example, cardiac contractility or ventricular preload, leading to unacceptable risks such as collapse of the left ventricle or impairment of the right heart function (2). For example, some patients implanted with IRBPs have reported feeling faint during postural changes, Valsalva maneuvers, coughing, or straining.

Interaction between IRBPs and the cardiovascular system (CVS) may be partially explored through in vivo animal studies (3–6). However, such studies are inconclusive at present due to limitations in animal models of heart failure and complexity of the experimental procedures (7). Numerical models able to simulate the response of the human CVS in the presence of an IRBP can provide additional insights into the dynamics of the assisted circulation. In particular, hemodynamic response to circulatory perturbations, such as cardiac contractility, ventricular preload, and afterload, has gained considerable interest in the field of IRBPs. Numerical models also offer an excellent platform for the development

and evaluation of robust physiological pump control algorithms by easily allowing reproducible numerical experiments under identical conditions.

Various heart–pump interaction models have been described in the literature, with varying degrees of complexity depending on their purpose. Complex models have been used to investigate the effect of IRBPs on hemodynamic response under various physiological conditions and under diverse control strategies (7–10). However, reduced models are often used for control algorithm development because of their faster computation time and lower number of parameters providing improved model identifiability (11–13). Morley et al. (14) examined the hemodynamic effects of partial left ventricular (LV) support using a computational model of the CVS, validated with data obtained from an acute in vivo preparation of chronic heart failure. However, Vollkron et al. (7) performed parameter variation studies on their numerical model to investigate the interaction between the pump and the heart under varying conditions, for example, pump speed, circulatory blood volume, heart frequency, and cardiac contractility, and compared their simulation results qualitatively with findings in the patients. One common limitation of the previous studies is that they have not focused on fitting the entire waveforms to actual experimental measurements obtained under various perturbations to the circulatory system, for example, variations in cardiac contractility and systemic vascular resistance (SVR) conditions. These variations are common in real-life scenarios and would create unacceptable risks to the patients if pump control was not properly implemented (2). Furthermore, some important parameters which are useful for IRBP control, for example, the pulsatility index, have shown dependencies on the physiological parameters such as contractility and afterload (15). Despite this, preliminary model validation efforts have focused mainly on a limited number of hemodynamic variables within a narrow operating range. To study the hemodynamic response under other operating conditions, these models were normally extrapolated. Due to the highly nonlinear nature of the model and the complexity of heart–pump interaction, this approach has led to considerable speculation.

Therefore, the aim of the present study is to develop an optimized heart–pump interaction model based on animal experimental measurements obtained from five canines over a wide range of operating conditions, including variations in pump speed (between 1250 rpm and 3000 rpm), cardiac contractility, SVR, total circulatory volume, V_{total}, and heart rate (between 70 and 130 bpm). These variations are

common in real-life scenarios and would create unacceptable risks to the patients if pump control is not properly implemented. Least squares parameter estimation methods are utilized to fit the parameters for the CVS and the pump cannulae in order to achieve better agreement with the experimental data and to evaluate the robustness and validity of the model under various operating conditions. The fitted model produced reasonable agreement with the experimental measurements, both in terms of mean values and steady-state waveforms. Furthermore, all the optimized parameters were within physiological limits.

METHODS

Animal experiments

Animal experiments were conducted in the Monash University, Department of Surgery, Alfred Hospital, over 3 consecutive months. Ethical approval for the animal experimentation work was given by the Alfred Medical Research and Education Precinct animal ethics committee.

The VentrAssist IRBP (Ventracor Ltd, Sydney, Australia) was acutely implanted in five healthy, anesthetized, open-chest dogs (greyhounds) supported by mechanical ventilation (average weight of 30 kg). The inflow cannula (10 mm in diameter and 10 cm in length) was inserted at the apex of the left ventricle and the outflow cannula (10 mm in diameter and 20 cm in length) anastomosed to the ascending aorta. The greyhounds were instrumented with indwelling catheters and pressure transducers connected to either a S/5 Light Monitor (Datex Ohmeda, Inc., Madison, WI, USA) or a Hewlett Packard Merlin Monitor (Philips Medical Systems, Inc., Bothell, WA, USA) to record the LV pressure (P_{lv}), left atrial (LA) pressure (P_{la}), aortic pressure (P_{ao}), vena cava pressure (P_{vc}), pulmonary arterial pressure (P_{pa}), pump inlet pressure (P_{in}), and pump outlet pressure (P_{out}). P_{lv} was measured at the proximal part of the left ventricle (below the mitral valve), P_{la} was measured at the left atrium, P_{in} was measured at the pump inflow cannula (near the inlet of the pump), while P_{out} was measured at the pump outflow cannula (near the outlet of the pump). Ultrasonic flow probes interfaced with a T106 flowmeter (Transonic Systems, Inc., Ithaca, NY, USA) were used to record flow rate across the aortic valve (Q_{av}) (with the perivascular flow probe placed around the ascending aorta, upstream of the anastomosis) and pump flow rate (Q_p). In addition, instantaneous pump impeller speed (ω), motor current (I), and supply voltage (V) were also recorded. A three-lead electrocardiogram

(ECG) signal and the animal's temperature were also monitored throughout the experiment.

During the experiment, arterial blood gas testing was performed approximately every 1 h to determine the pH of the blood, the partial pressure of carbon dioxide and oxygen, the bicarbonate level, the concentrations of lactate, hemoglobin (which determines blood viscosity), and several electrolytes. A cardiotomy suction system was used for recovering blood loss from the animal throughout the experiment, as well as for varying total blood volume in the animal's circulation during preload dependence studies. Syringe pumps were used to administer specific drugs at a controlled rate during the afterload dependence studies. A pacemaker was used during the last two experiments (two out of five greyhounds) to maintain a constant heart rate throughout the experiment, particularly to counter the bradycardic effect caused by application of beta-blockers. The measured signals, including Q_{av}, Q_p, P_{ao}, P_{lv}, P_{la}, P_{vc}, P_{pa}, P_{in}, P_{out}, CO, ω, I, V, and ECG were continuously recorded and displayed on a laptop using the Powerlab Data Acquisition System with the Chart 5 software (ADInstruments Pty Ltd., Sydney, Australia). The sampling rate of the data acquisition system was set to 4 kHz.

Each animal experiment was started with a speed ramp study for "healthy condition" ($H1$), where the pump outflow cannula was first occluded to record the baseline hemodynamic variables. The occlusion was then released and the impeller speed set point was increased from 1250 rpm to the speed when suction occurred, in 100 rpm increments. At each speed, all the recorded variables were ensured to reach steady state before proceeding to the next speed. At the end of the speed ramp run, pump speed was turned down to 1600 rpm, and a blood sample was taken for blood gas analysis purposes.

This was followed by the administration of a cardiodepressant, beta1-receptor blocker drug (Metoprolol) through the venous line to decrease the inotropic state of the heart. Metoprolol is a beta-adrenergic blocking agent, which reduces or inhibits the stimulant effect of catecholamines on the heart, leading to a decrease in heart rate, cardiac contractility, and cardiac output (CO). The drug was injected in small amounts (up to 5 mg) to avoid excessive hemodynamic responses. After each bolus of injection, a short period of time was needed to allow the hemodynamic variables to reach their steady-state levels. The pump outflow cannulae were then occluded to determine the baseline CO. Further injection of the beta-blocker was performed until either the baseline CO reached 50% of the "healthy condition" or until

the P_{ao} dropped below 60 mm Hg at a speed of 1600 rpm. A speed ramp study for the "reduced heart contractility condition—afterload low" ($H2$) was performed once all the hemodynamic variables reached their steady-state levels.

This was followed by the afterload dependence studies. Afterload was increased by the administration of Metaraminol (solution containing 10 mg Metaraminol diluted in 20 mL of fluid), a potent sympathomimetic drug with a vasoconstrictive action. Metaraminol acts mainly on the resistance vessels through the peripheral alpha-adrenergic receptors, leading to an increase in the systolic and diastolic blood pressure, thus raising the afterload as seen by the ventricle. Apart from the vasoconstrictive effect, it also has a minor effect on heart contractility and heart rate through the beta-adrenergic receptors, as well as causing venoconstriction and pulmonary vasoconstriction. Its effect begins in 1 to 2 min after intravenous infusion and tapers off gradually within 20 min to 1 h after the drug is discontinued. Therefore, during a speed ramp run for each of the afterload dependence tests, consistency of afterload was ensured by continuous administration of Metaraminol at a fixed rate using a syringe pump (the actual infusion rate varied widely in different animals, from 1.5–3 μg/kg/min, depending on its effect on each animal). The infusion rate was first adjusted to increase the mean P_{ao} ($\overline{P_{ao}}$) approximately 20 mm Hg higher compared with case $H2$, at a speed of 1600 rpm. Once this was reached and after all hemodynamic variables were stabilized, a speed ramp study for the "reduced heart contractility condition—afterload medium" ($H3$) was performed. This was repeated for another level of afterload ("reduced heart contractility condition—afterload high" or $H4$), at a $\overline{P_{ao}}$ of 20 mm Hg higher compared to case $H3$. In case of excessive increase in blood pressure caused by the infusion of Metaraminol, the vasodilator sodium nitroprusside was administered (solution containing 30 mg Metaraminol diluted in 50 mL of fluid). Sodium nitroprusside breaks down in the blood and releases nitric oxide, which then enters the muscle cells in the walls of the blood vessels and causes them to relax. Similar to Metaraminol, the actual infusion rate for the sodium nitroprusside also varied widely in different animals, from 15 to about 30 μg/kg/min, depending on its effect on each animal.

This was followed by the preload dependence tests, where the rate of the cardiotomy suction system was varied in order to change the total blood volume. Before starting these tests, the syringe pump was turned off to stop the infusion of Metaraminol. After all the hemodynamic variables had stabilized, a speed

ramp test ("reduced heart contractility condition —preload low" or $H5$) was performed. This was repeated for two other volume levels ("reduced heart contractility condition—preload medium" or $H6$ and "reduced heart contractility condition—preload high" or $H7$) by changing the rate of the cardiotomy suction machine. Gelofusine, which has a higher osmolarity than plasma, was used as the fluid medium to reduce the rate of blood volume leakage into the interstitial tissue. Stability was assumed to be achieved when central venous pressure (P_{vc}) and volume in the venous reservoir chamber of the cardiotomy suction machine remained constant for at least 20 min.

At the end of the procedure, but while the animal remained anesthetized, a precalculated IV bolus of ethanol was used to terminate the experiment. All drainage cannulae were visually checked and no mobile obstructing tissue was detected at the cannulae orifice.

Heart–pump interaction model

The model presented in this paper is a modification of our previous model (16). The heart–pump interaction model consists of two main components, that is, the CVS and the left ventricular assist device (LVAD). The lumped parameter CVS component includes 10 compartments consisting of the pulmonary and systemic circulations as well as the left and right sides of the heart. The LVAD component includes the description of the IRBP, as well as the inlet and outlet cannulae. A detailed description of the model can be obtained from reference (16).

In the present study, a number of model features which have not been included in the existing heart–pump interaction models were incorporated to accurately reproduce the experimental data obtained over a much wider range of operating points, for example, wide range of pump speeds (which cover different cardiac pumping states: ventricular ejection [VE], i.e., when $Q_{av} > 0$, nonopening of the aortic valve over the whole cardiac cycle (ANO), i.e., when $Q_{av} = 0$, and ventricular suction [SUC]), heart contractilities, preload, and afterload. These include nonlinear pressure volume relationship of the aorta and vena cava compartments, nonlinear pulmonary peripheral resistance, and piecewise function for the pump cannula model.

Nonlinear pressure volume relationship

As the present data include a wide range of pressure values (P_{ao} within a range of 32–175 mm Hg and P_{vc} within a range of 0–26 mm Hg), nonlinear pressure volume relationships were adopted for both the aorta and vena cava (17), as follows:

$$P_{ao} = A_{ao}(V_{ao} - V_{0,ao})^2 \tag{1}$$

$$P_{vc} = P_{0,vc}\left(e^{\lambda_{vc}(V_{vc} - V_{0,vc})} - 1\right) \tag{2}$$

where A_{ao}, $V_{0,ao}$, $P_{0,vc}$, λ_{vc}, and $V_{0,vc}$ are constants.

Description of pulmonary peripheral resistance

Our experimental observations revealed a high correlation between pulmonary vascular resistance (PVR, mainly determined by pulmonary peripheral resistance, R_{pa}) and $\overline{P_{la}}$. The experimental results showed that when $\overline{P_{la}}$ dropped below a threshold value (~6 mm Hg), PVR increased exponentially with a decrease in $\overline{P_{la}}$. As pressure downstream of the pulmonary peripheral vessel, P_{pu}, is closely related to $\overline{P_{la}}$, R_{pa} was modeled as a function of P_{pu} (i.e., the downstream pressure):

$$R_{pa} = \begin{cases} A_{pa} + B_{pa}e^{-C_{pa}P_{pu,th}} & P_{pu} \geq P_{pu,th} \\ A_{pa} + B_{pa}e^{-C_{pa}P_{pu}} & P_{pu} < P_{pu,th} \end{cases} \tag{3}$$

where A_{pa}, B_{pa}, and C_{pa} are constants, P_{pu} represents the pressure downstream of the pulmonary peripheral vessel, while $P_{pu,th}$ represents the threshold of P_{pu} below which PVR increased exponentially with a decrease in P_{pu}.

Pump cannula model

Various cannulae formulations were fitted to the experimental data (Q_p between –5 and 9 L/min), including the P_{lv}, P_{in}, P_{out}, P_{ao}, Q_p, and pump speed. Results revealed that during regurgitant Q_p ($Q_p < 0$), cannula resistance can be assumed to be constant, with a higher magnitude compared to that in the positive Q_p region. However, the experimental results showed that while the cannula resistance can be assumed to be constant during low positive Q_p ($0 \leq Q_p < Q_{p,r}$, where $Q_{p,r}$ is an experimentally fitted constant value), it is best modeled as an increasing function of Q_p in higher positive flow regions ($Q_p \geq Q_{p,r}$), due to the transition of flow characteristics from laminar to turbulent:

$$R_{in} + R_{out} = \begin{cases} k_{R,n} & Q_p < 0 \\ k_{R,p} & 0 \leq Q_p < Q_{p,r} \\ k_{R,p} + k_{R2,p}(Q_p - Q_{p,r})^{0.7} & Q_p \geq Q_{p,r} \end{cases} \tag{4}$$

where $k_{R,n}$, $k_{R,p}$, $k_{R2,p}$, and $Q_{p,r}$ are constants. Using the proposed cannula model, we were able to achieve goodness of fit (R^2 value) of 0.94.

Computational aspects

Each animal experiment consisted of seven speed ramp tests, that is, the control state ("healthy condition") and the reduced cardiac contractility states which included the three different afterload conditions and the three different preload conditions. In order to investigate the effect of the above-mentioned perturbations (heart contractility, afterload and preload) on heart–pump interaction, the results from all the five animals were grouped and divided according to the seven categories and pump speeds. Mean and standard deviation of the measured or derived variables, for example, the pulsatility index or the amplitude of the corresponding signals (PI), pulse pressure, PVR, and SVR from each category at each pump speed were calculated and plotted to represent (i) heart contractility dependence; (ii) afterload dependence; and (iii) preload dependence.

Using the modified heart–pump interaction model, the model parameters used for the healthy human circulation were first scaled to that of a healthy adult greyhound, which has a lower blood volume, that is, approximately 3400 mL. The model parameters were then optimized to reproduce pressure, flow, and volume distributions in a healthy greyhound circulation. In order to examine if the model could qualitatively predict the observed changes in the measured variables caused by a specific perturbation on the CVS, a subset of parameters in the model were changed according to the effect of the corresponding perturbations. To simulate the effect of Metoprolol, model parameters which described the linearized left and right ventricular (RV) end-systolic pressure volume relationship (ESPVR) ($E_{es,lvf}$ and $E_{es,rvf}$) were decreased. To simulate the effects of Metaraminol or sodium nitroprusside on the CVS, model parameters which corresponded to the resistance of the systemic and pulmonary peripheral vessels (R_{sa} and A_{pa}), linearized LV and RV ESPVR ($E_{es,lvf}$ and $E_{es,rvf}$), and systemic vein unstressed volume ($V_{0,sv}$) were modified. To simulate exsanguination and the volume loading effects of Gelofusine, the parameter which represented the total circulatory volume (V_{total}) was modified. Resulting simulation results of the various perturbations were compared qualitatively to the experimental measurements.

If the model qualitatively reproduced the trends observed in the experiments, the next step, which was to optimize the model parameters to reproduce individual experimental datasets in a quantitative sense, was carried out using the methods described in the previous paper (16). The optimization process was carried out separately for each animal. It consisted of

data obtained at seven different conditions ($H1$, $H2$, $H3$, $H4$, $H5$, $H6$, and $H7$). All the waveform measurements from half of the speed settings in each perturbation were used in the optimization process to search for parameter values which minimized the objective function, defined by

$$F = \Sigma_i w_i (y_{model,i}(\theta) - y_{meas,i})^2 \qquad (5)$$

where w_i denotes the weight corresponding to the ith experimental dataset, including P_{lv}, P_{la}, P_{ao}, P_{vc}, P_{pa}, P_{in}, P_{out}, Q_{av}, Q_p, ω, and I. w_i was determined so that each experimental dataset initially contributed equally to the least-squares objective. θ represents model parameters, $y_{model,i}$ denotes the ith model output, while $y_{meas,i}$ denotes the ith experimental measurement corresponding to the ith model output. Data from other speed settings were used to test the predictability of the model in describing data that was not used in the fitting process. We ensure that data for both the fitting and testing process cover a wide range of rotational speeds.

Out of the 82 model parameters, 32 parameters were chosen to be included in the nonlinear least squares parameter estimation algorithm, while values of the remaining parameters were fixed and shared by all the animals. These parameters were chosen using the sensitivity analysis approach described in (16). In order to fully describe the experimental measurements by only optimizing the necessary parameters which are known to change, among the 32 parameters, the values of 20 of these ($V_{0,lvf}$, $P_{0,lvf}$, λ_{lvf}, $V_{0,rvf}$, $P_{0,rvf}$, λ_{rvf}, A_{ao}, $V_{0,ao}$, E_{sv}, $P_{0,vc}$, λ_{vc}, $V_{0,vc}$, E_{pa}, E_{pu}, R_{av}, R_{ao}, $k_{R,p}$, $k_{R2,p}$, $k_{R,n}$, and $Q_{p,r}$) were shared by all the seven operating conditions.

Eleven parameters related to LV and RV contractilities ($V_{d,lvf}$, α_{lvf}, β_{lvf}, $V_{d,rvf}$, α_{rvf}, and β_{rvf}), systemic and peripheral resistances (R_{sa}, A_{pa}, B_{pa}, and C_{pa}), as well as systemic vein unstressed volume ($V_{0,sv}$) were individually estimated in $H1$ to $H5$ to simulate the effect of Metoprolol or Metaraminol. The remaining parameter, V_{total}, was assumed to be shared by all these five conditions. On the contrary, $H5$, $H6$, and $H7$ were assumed to share the same values for all parameters except V_{total}. Therefore, a total of 78 parameters were estimated for each animal using the experimental measurements for the corresponding animal under various operating conditions.

Before running the optimization algorithm, measurements of P_{in}, P_{out}, P_{lv}, P_{ao}, Q_p, pump speed, pump current, and blood viscosity level were used to provide initial estimates of model parameters related to the pump and cannula.

Measurements of $\overline{P_{ao}}$, mean P_{vc} ($\overline{P_{vc}}$), mean P_{pa} ($\overline{P_{pa}}$), mean LA pressure ($\overline{P_{la}}$), and mean cardiac output ($\overline{CO}$) were used to estimate the initial values for SVR and PVR in each dataset, that is,

$$SVR(mm\ Hg.s/mL) = \frac{\overline{P_{ao}} - \overline{P_{vc}}}{\overline{CO}} \qquad (6)$$

$$PVR(mm\ Hg.s/mL) = \frac{\overline{P_{pa}} - \overline{P_{la}}}{\overline{CO}} \qquad (7)$$

A constant heart rate, estimated from the ECG during the experiments, was used as an input to run the model. The input to the model which was varied during each speed variation is the measured pulse-width modulated voltage signal to the pump. The optimization process was restarted several times with different initial estimates to search for the best set of parameters which minimized the objective function, *F.* Values for the optimized parameters for each greyhound are given in Tables A1–A3. Mean values of the optimized parameters over all the five animals were also listed in the tables.

In order to estimate the quantitative confidence limits on the fitted parameters, we computed standard deviations of the individual parameters by performing Monte-Carlo simulations using synthetic datasets. First, we calculated the "measurement error," taken as the root mean square value (RMS) of the error between our experimental results and the model output generated using the fitted parameters. Then, 10 different sets of synthetic data were generated at each data point ($y_{synthetic,i}$) for each greyhound, using the following equation:

$$y_{synthetic,i} = y_{model,i} + error * randn \qquad (8)$$

where *randn* is a series of normally distributed variables of mean 0 and standard deviation 1. Using these synthetic datasets, we then performed the optimization process, starting from the same initial model parameters (i.e., the fitted values) to obtain the newly fitted parameters. The distribution of these newly fitted parameters around the original parameters (i.e., the standard deviation of the individual parameters) can then be obtained. All standard deviations were less than 1% of the fitted parameter values, except those indicated in Tables A2 and A3.

RESULTS

Table 1 shows the RMS value of the error and the goodness of fit (R^2) between the experimental data and the simulation results for all five greyhounds after optimization. It can be seen that the model fitting process produced a reasonably good agreement in all variables between the experimental measurements and the model simulations (with an error of less than 10%, except for P_{la} and P_{vc}, which has an error of less than 20%). The negative value of R^2 for P_{la} in greyhound 1 is due to the fact that although the mean values of P_{la} in the simulation results were close to that obtained from the experiments, the waveforms were out of phase with each other.

Effect of beta-blocker (ventricular contractility)

Figure 1 illustrates waveforms of one of the greyhound experiments (greyhound 2) superimposed on the model simulations before and after the injection of beta-blocker (*H*1 and *H*3 conditions), under pump occlusion and different pump speed settings. Both the experimental and simulation results, as well as the optimized model parameters which described the LV and RV ESPVR (Table A3), agreed with the expected effect of the beta-blocker, that is, a decrease in heart rate and cardiac contractility.

TABLE 1. *Root mean square (RMS) value of the error and the goodness-of-fit (*R²*) between the experimental data and the simulation results using the optimized parameters*

Measurements	Range	Dog 1		Dog 2		Dog 3		Dog 4		Dog 5	
		Error	R^2	Error	R^2	Error	R^2	Error	R^2	Error	R^2
P_{lv} (mm Hg)	−3–160	7.83	0.97	10.76	0.92	10.40	0.91	6.02	0.97	13.20	0.84
P_{la} (mm Hg)	−3–33	5.14	−0.04	3.70	0.35	4.36	0.68	2.79	0.73	4.57	0.49
P_{ao} (mm Hg)	32–175	5.67	0.94	6.50	0.93	6.61	0.94	4.17	0.97	6.00	0.95
P_{pa} (mm Hg)	5–40	2.90	0.73	3.80	0.70	3.25	0.78	3.11	0.74	3.00	0.74
P_{vc} (mm Hg)	0–26	0.55	0.16	1.17	0.19	1.29	0.43	3.85	0.37	2.26	0.57
Q_p (L/min)	−5–9	0.61	0.91	0.73	0.93	0.47	0.94	0.45	0.95	0.97	0.81
Q_{av} (L/min)	−4–35	2.50	0.84	1.38	0.72	1.79	0.67	2.25	0.59	1.71	0.42
ω (rpm)	1250–3000	29.88	0.99	65.69	0.96	27.77	1.00	23.77	1.00	35.55	0.99
I (A)	0.05–0.9	0.01	0.97	0.05	0.71	0.03	0.94	0.01	1.00	0.01	0.98

The R^2 value was calculated using $R^2 = 1 - \Sigma(y_{meas} - y_{model})^2 / (y_{meas} - \overline{y_{meas}})^2$. y_{meas} represents the experimental measurements, y_{model} represents the model outputs, while $\overline{y_{meas}}$ represents the mean value of the experimental measurements.
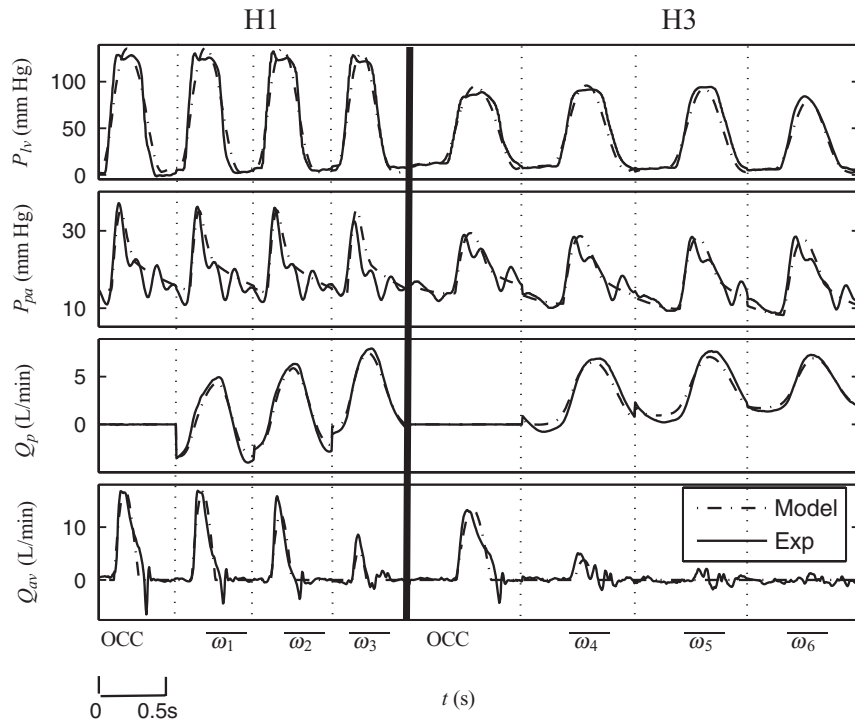
FIG. 1. Left ventricular pressure (P_{lv}), pulmonary arterial pressure (P_{pa}), aortic valve flow (Q_{av}), and pump flow (Q_p) waveforms from an in vivo greyhound experiment (greyhound 2) implanted with an IRBP superimposed on model simulations with the IRBP operating with pump occlusion (OCC) and at different pump speed settings (i.e., $\overline{\omega_1}$ = 1500 rpm, $\overline{\omega_2}$ = 1800 rpm, $\overline{\omega_3}$ = 2100 rpm, $\overline{\omega_4}$ = 1800 rpm, $\overline{\omega_5}$ = 2000 rpm, $\overline{\omega_6}$ = 2200 rpm), before (*H*1) and after (*H*3) the injection of a beta-blocker. During pump occlusion, the pump outflow cannula was occluded to record the baseline hemodynamic variables.

Compared with the healthy heart condition (*H*1), we observed a decrease in the P_{ao}, P_{pa}, and CO ($Q_p + Q_{av}$), as well as an increase in P_{vc} and P_{la} under depressed cardiac contractility conditions (*H*3). A dicrotic notch could be clearly seen in the P_{ao} waveform during the VE state. Simulation results showed a high degree of correlation with the experimental data, both in terms of mean values and response dynamics. However, the model was not able to reproduce the regurgitant Q_{av} phase at the end of ejection due to the use of an ideal valve model.

One important observation from our experimental measurements is that during speed ramp studies under normal LV contractility conditions (*H*1) with high stroke volume (*SV*) and low LV end-systolic volume ($V_{lv,es}$), suction occurred temporarily within each heartbeat before full LV decompression (or *ANO* state), that is, when maximum P_{lv} ($P_{lv,max}$) was still relatively high. SUC was detected by monitoring apical intraventricular pressure (or P_{in}) as well as Q_p. Collapse of the ventricle was evident from observation of the Q_p and P_{in} waveforms, which showed a transient reduction when the ventricular walls suck together. This occurred near the point of end systole, that is, shortly after P_{lv} reached its maximum value in the cardiac cycle. In most cases, partial occlusion of the inlet cannula occurred, causing modest reduction in Q_p (Fig. 2). Severe suction occurred infrequently at high pump speeds and was associated with transient

complete occlusion of the pump inlet cannula causing LVAD flow to fall to zero and P_{in} to fall to a pressure of <−80 mm Hg.

Effect of Metaraminol or sodium nitroprusside (systemic afterload)

Figure 3 illustrates the effect of Metaraminol or sodium nitroprusside infusion on the waveforms of one of the greyhound experiments (greyhound 4) superimposed on the model simulations using the optimized parameters for that greyhound (*H*2–*H*4 conditions), under various pump speed settings. Both the experimental and simulation results (greyhounds 1, 2, 4, and 5) agreed with published findings regarding the effect of Metaraminol (vasoconstriction and increased heart contractility) and sodium nitroprusside (vasodilatation). This was indicated by the optimized model parameters (Table A3) which describe the systemic peripheral resistance (R_{sa}) and the LV and RV ESPVR (α_{lvf}, β_{lvf}, $V_{d,lvf}$, α_{rvf}, β_{rvf}, and $V_{d,rvf}$ and the linearized parameters, i.e., $E_{es,lvf}$, $V_{d,lvf,lin}$, $E_{es,rvf}$, and $V_{d,rvf,lin}$). In all greyhounds, there was an increase in $E_{es,lvf}$ and R_{sa} from *H*2 to *H*4 which indicated increased LV contractility and SVR. On the contrary, there were no significant variations in the pulmonary peripheral resistance parameters (A_{pa}, B_{pa}, and C_{pa}) from *H*2 to *H*4. In three out of four greyhounds (greyhounds 1, 4, and 5), there was an increase in
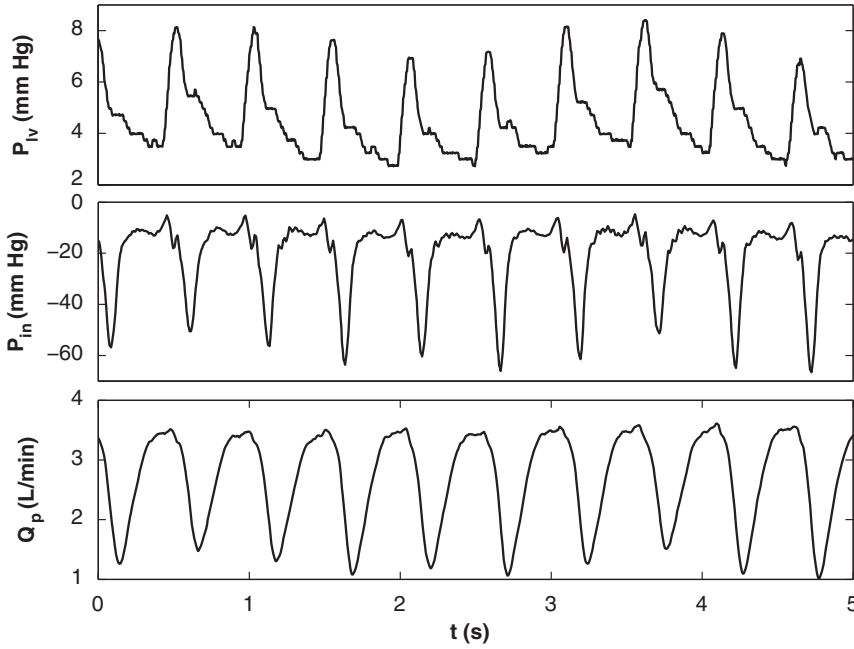
FIG. 2. Time course of LV pressure, P_{lv}, pump inlet pressure, P_{in}, and pump flow, Q_p from one of the greyhound experiment (greyhound 4) implanted with IRBP during LV suction caused by an excessive pump speed setting.

$E_{es,rvf}$ and a decrease in $V_{0,sv}$ from $H2$ to $H4$, which is indicative of increased RV contractility and venoconstriction.

Increasing LV and RV contractilities, as well as the SVR from $H2$ to $H4$, led to a significant increase in the P_{lv}, P_{ao}, RV pressure (P_{rv}), and CO. The large increase in P_{ao} imposed a high afterload on the left ventricle, leading to an increase in P_{la} and P_{pa}. Fur-

thermore, regurgitant Q_p, which increases volume loading on the left ventricle, can also be observed at high afterload pressures for lower pump speeds. Simulation results showed a high degree of correlation with the experimental data in all pressure, flow, and pump waveforms, except for Q_{av}. We observed small positive Q_{av} in the experimental results during diastole when it should be zero, as physiologically the
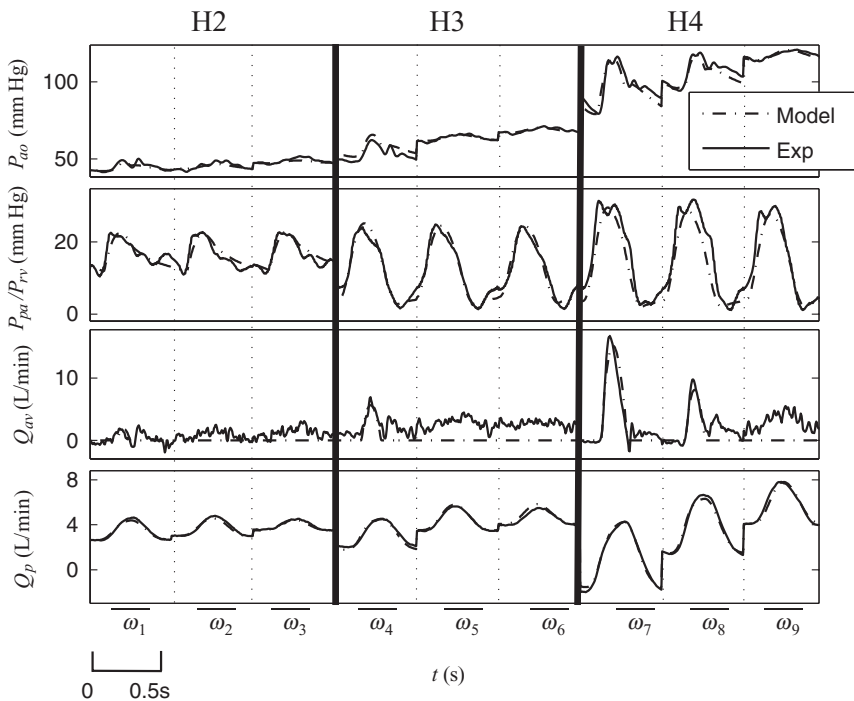
FIG. 3. Aortic pressure (P_{ao}), pulmonary arterial pressure (P_{pa})/RV pressure (P_{rv}), aortic valve flow (Q_{av}), and pump flow (Q_p) waveforms from an in vivo greyhound experiment (greyhound 4) implanted with an IRBP, superimposed on model simulations with the pump activated at different speed settings (i.e., $\overline{\omega}_1$ = 1600 rpm, $\overline{\omega}_2$ = 1700 rpm, $\overline{\omega}_3$ = 1900 rpm, $\overline{\omega}_4$ = 1600 rpm, $\overline{\omega}_5$ = 2000 rpm, $\overline{\omega}_6$ = 2200 rpm, $\overline{\omega}_7$ = 1600 rpm, $\overline{\omega}_8$ = 2100 rpm, $\overline{\omega}_9$ = 2600 rpm), under sodium nitroprusside ($H2$) or Metaraminol ($H3$ [lower infusion rate] and $H4$ [higher infusion rate]) infusion. P_{rv} was obtained in the $H3$–$H4$ conditions instead of P_{pa} due to temporary dislocation of the Swan Ganz catheter during the experiment.
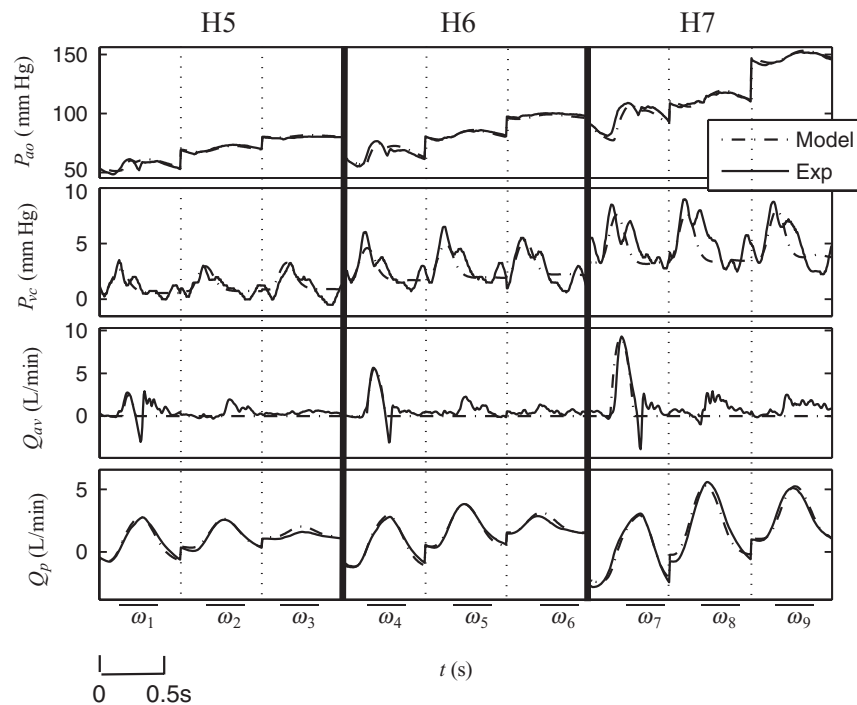
FIG. 4. Aortic pressure (P_{ao}), vena cava pressure (P_{vc}), aortic valve flow (Q_{av}), and pump flow (Q_p) waveforms from an in vivo greyhound experiment (greyhound 3) implanted with an IRBP, superimposed on model simulations with the IRBP activated at different pump speed settings (i.e., $\overline{\omega_1}$ = 1400 rpm, $\overline{\omega_2}$ = 1800 rpm, $\overline{\omega_3}$ = 2100 rpm, $\overline{\omega_4}$ = 1400 rpm, $\overline{\omega_5}$ = 1900 rpm, $\overline{\omega_6}$ = 2300 rpm, $\overline{\omega_7}$ = 1400 rpm, $\overline{\omega_8}$ = 2000 rpm, $\overline{\omega_9}$ = 2600 rpm) and blood volume levels (H5 [volume low], H6 [volume medium] and H7 [volume high]).

aortic valve is closed during the diastole phase (when $P_{lv} < P_{ao}$). Therefore, we believe that this was an experimental artifact caused by turbulence in the aortic root.

Effect of volume loading using Gelofusine (preload)

Figure 4 illustrates the effect of total blood volume on the waveforms of one of the greyhound experiments (greyhound 3) superimposed on the model simulations using the optimized parameters for that greyhound (H5–H7 conditions), under different pump speed settings. The optimized parameter which describes the total blood volume, V_{total}, showed consistent results with the experiments (greyhounds 2–5), increasing in value from H5 to H7 (Table A3).

Increasing blood volume increased preload to both ventricles (as indicated by a significant increase in P_{la} and P_{vc}), leading to a substantial increase in P_{lv}, P_{ao}, P_{pa}, and CO. The effect of increasing blood volume on the hemodynamic response is similar to that of Metaraminol, except that increasing blood volume produced a much higher increase in vena cava (P_{vc}) and pulmonary arterial (P_{pa}) pressures. High pulsatility was observed in the P_{vc} waveform, especially at higher pump speeds, probably due to increased stiffness of the vessel at relatively high pressure. Simulation results showed a high degree of correlation with the experimental data, including pressure, flow, and

pump waveforms, both in terms of mean values and response dynamics. However, the model was not able to accurately reproduce the corresponding dynamics in P_{la} and P_{vc}, as the waveforms were corrupted by relatively higher levels of measurement noise, partly due to their lower absolute values as well as the improper positioning of the pressure transducers.

In terms of vascular resistance, both experiment and model simulations (Fig. 5) revealed an increase in PVR with increasing mean pump speed and decreasing V_{total}, despite a relatively constant SVR, due primarily to a decrease in pulmonary venous pressure (indicative of decreasing pulmonary blood volume).

DISCUSSION

In the present study, we have developed an optimized heart pump interaction model using experimental measurements obtained over a wide range of operating conditions. This systematic approach increases the robustness and validity of the model. However, as inherent in all nonlinear modeling problems, results of our parameter fitting process may not be unique or optimal, that is, we may have only found a local minimum. Uniquely determining all parameters would likely require isolated experiments for each compartment, measurements of different variables at many points in the circulation, as well as
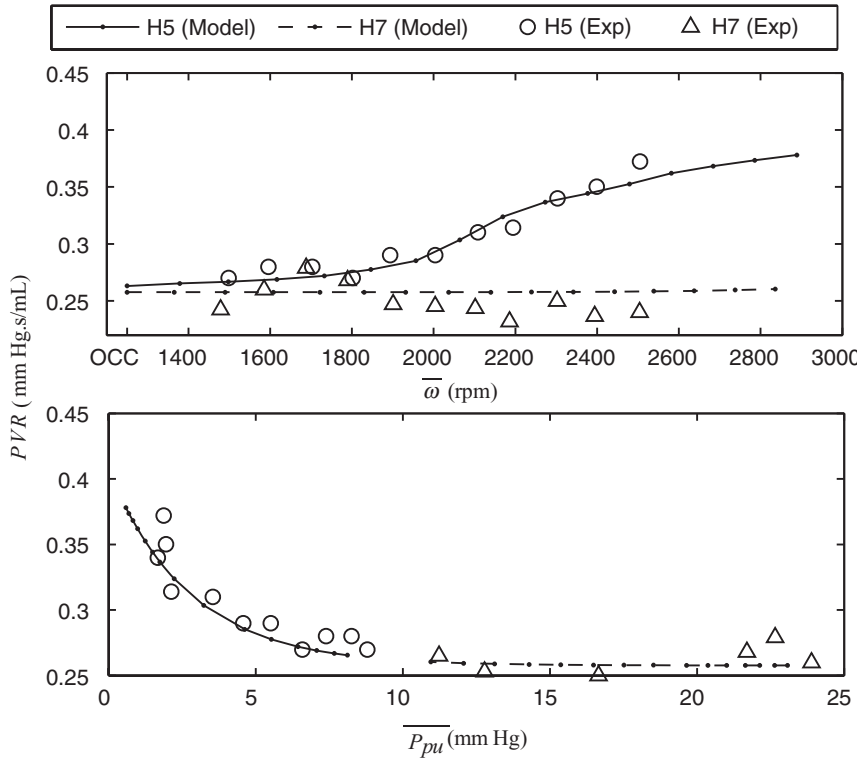
FIG. 5. (Top): Effect of mean pump speed ($\overline{\omega}$) and V_{total} on PVR from an in vivo greyhound experiment (greyhound 3) superimposed on model simulations at different blood volume levels ($H5$ [volume low]) and $H7$ [volume high]). (Bottom): Relationship between pulmonary peripheral resistance (R_{pa}) and pulmonary venous pressure (P_{pu}).

various well-controlled and measurable perturbations such as preload, afterload, heart rate, and heart contractility. However, given the goodness of fit between the model and the large amount of data at various pump speeds and circulatory conditions, and that it predicts data that were not used in the fitting process, we believe that the model is a valid representation of the system. In order to ensure that the optimized parameters are within physiological limits, we have also set constraints for each parameter at a reasonable range, starting at initial estimates obtained from well-established results in the literature.

As reported in the literature (18,19) and observed in our experimental and simulation results, $\overline{P}_{ao}$ and CO were not significantly changed by pump speed under normal LV contractility. One interesting observation from our experiments (in all greyhounds) is that the calculated SVR decreased with increasing mean pump speed for the healthy condition ($H1$), but was relatively constant during the speed ramp study under reduced cardiac contractility ($H2$–$H7$). The observed decrease in SVR for the healthy condition may be explained by previous experimental findings (19) which suggested that in the case of a recovering or healthier left ventricle, alternative Starling behavior (i.e., the autoregulatory mechanisms which cause

a change in the inotropic state of the heart, vascular resistance, and vascular tone) acts to preserve the overall CO required by the circulatory system, despite a decrease in end-diastolic volume and stroke volume. Furthermore, it is observed from our experimental measurements that during speed ramp studies under healthy LV conditions, LV suction occurred temporarily during end systole at pump speeds before full LV decompression (or ANO state), that is, when $P_{lv,max}$ was still relatively high. This is because at relatively high cardiac contractility, the left ventricle ejects a large amount of blood during systole, leading to low LV end-systolic volumes.

We also observed an increase in PVR under low circulatory volume, low SVR, and high pump speed conditions (Fig. 5). One common feature shared by these three conditions is low mean P_{la} (below a threshold value of ~6 mm Hg), which reflected low pulmonary blood volume. An increase in PVR limits venous return to the left ventricle while increasing pulmonary afterload, leading to an earlier transition into suction. Consequently, there is a relatively lower augmentation of CO with increasing mean pump speed under these conditions. Moreover, Reesink et al. have suggested that suction-induced vessel collapse is responsible for the persistence of collapse after a suction event (20).

In regard to the cannula model, our results revealed that during regurgitant Q_p, cannula resistance can be assumed to be constant, with a higher magnitude compared to that in the positive Q_p region. However, the experimental results showed that while the cannula resistance can be assumed to be constant during low positive Q_p, it is best modeled as an increasing function of Q_p in higher positive flow regions. The flow-dependent resistance could be explained by a gradual transition of laminar flow into turbulence, altering the effective cannula resistance. This feature is also partly responsible for the nonlinear increase of Q_p with increasing pump speed, with lower increases at higher pump speeds.

Model limitations

The objective of this study was to develop a single set of model equations, albeit with considerable nonlinear terms and interactions, to sufficiently describe the complexity of the heart–pump interaction in any given subject. We envisage that each subject, each with unique physiologic condition, would be characterized by their own set of model parameters. Therefore, our proposed model would require optimization for each specific patient. Nonetheless, the model is a powerful predictor of heart–pump interaction over a wide range of operating conditions.

The model was not able to accurately reproduce the corresponding dynamics in P_{la} and P_{vc} in greyhounds 1 and 2 (reflected by poor R^2 values), although with reasonable fits in terms of the mean values. This is because the waveforms were corrupted by relatively higher levels of measurement noise, partly due to their lower absolute values as well as the improper positioning of the pressure transducers. Furthermore, the model was not able to reproduce the regurgitant Q_{av} phase at the end of ejection due to the use of an ideal valve model.

The present study used a beta-blocker to reduce cardiac contractility in the greyhounds to represent acute heart failure. The half-life of the drug is 3 to 7 h, which exceed the total duration of each experiment. Different greyhounds have very different responses to the beta-blocker, that is, some of the greyhounds are very sensitive to the drug (small dose created severe heart failure which may cause cardiac arrest), while others are not. Due to this reason, as well as the long half-life duration of the beta-blocker, continuous administration of the drug was not performed throughout the experiment. Instead, careful precautions were taken during the experiments, for example, the level of blood pressure and CO was checked before each speed ramp test to make sure that the heart's functional parameters were indicative of a "relatively" weak state.

Furthermore, it has been reported that the hemodynamic responses of the cardiovascular–rotary blood pump system may be different under chronic heart failure conditions (5). For example, sodium and water retention is frequently observed in chronic heart failure patients but not in acute heart failure patients, due to the actions of the compensatory mechanisms involved in regulating the CO. In addition, cardiomegaly (enlarged heart) occurs in chronic heart failure conditions but not necessarily in patients with acute heart failure (21). Therefore, further experimental studies using animals with induced chronic heart failure should be carried out to more accurately represent the actual clinical scenario.

In the present study, real-time LV volume measurements were not obtained due to limitation of the equipment availability as well as the technical complexity of in situ real-time ventricular volume measurements. As a result, important features such as the ventricular interaction model under VAD assistance, as well as the model parameters related to the time-varying elastance model and the ventricular chambers could not be accurately identified. Further experiments which measure instantaneous LV pressure and volume under various loading conditions are needed to better validate the model and more accurately identify the model parameters, particularly those closely related to the ventricular chambers.

The present model does not incorporate the autonomic reflex control mechanisms, which have been shown to be important under conditions of heart failure (22) and exercise (23), due to their complexity. Further extension of our model to incorporate the reflex control system is needed to simulate these pathological conditions. However, careful attention would have to be taken while modeling the autonomic reflex mechanisms based on existing observations reported in the literature using normal subjects, as reports have shown that the reflex response in a chronic heart failure patient may be significantly different from that of a healthy subject (22).

CONCLUSION

The work herein introduces a detailed and systematic approach in developing an optimized heart–pump interaction model based on experimental data obtained over a wide range of operating conditions,

including variations in pump speed, cardiac contractility, SVR, total circulatory volume, and heart rate. Simulated responses of the model under various operating points were quantitatively compared to experimental data, both in terms of mean values and steady-state waveforms. The heart–pump interaction model can be used as (i) a predictive tool for various studies, for example, response to exercise and postural changes; (ii) a platform for the evaluation of robust physiological pump control algorithms; and (iii) a tool to study the correlation between physiological variables and noninvasive variables under various conditions. If an optimal control method for an LVAD is to be built using this model, it has to be reduced to a simplified version with a smaller number of parameters.

REFERENCES

1. Park SJ, Tector A, Piccioni W, et al. Left ventricular assist devices as destination therapy: a new look at survival. *J Thorac Cardiovasc Surg* 2005;129:9–17.
2. Vollkron M, Schima H, Huber L, Benkowski R, Morello G, Wieselthaler G. Development of a reliable automatic speed control system for rotary blood pumps. *J Heart Lung Transplant* 2005;24:1878–85.
3. McConnell PI, Del Rio CL, Kwiatkowski P, Farrar DJ, Sun BC. Assessment of cardiac function during axial-flow left ventricular assist device support using a left ventricular pressure-derived relationship: comparison with pre-load recruitable stroke work. *J Heart Lung Transplant* 2007;26:159–66.
4. Moon MR, Castro LJ, DeAnda A, Daughters GT, Ingels NB, Miller DC. Effects of left ventricular support on right ventricular mechanics during experimental right ventricular ischemia. *Circulation* 1994;90:92–101.
5. Goldstein AH, Monreal G, Kambara A, et al. Partial support with a centrifugal left ventricular assist device reduces myocardial oxygen consumption in chronic, ischemia heart failure. *J Card Fail* 2005;11:142–51.
6. Akimoto T, Yamazaki K, Litwak P, et al. Rotary blood pump flow spontaneously increases during exercise under constant pump speed: results of a chronic study. *Artif Organs* 1999;23:797–801.
7. Vollkron M, Schima H, Huber L, Wieselthaler G. Interaction of the cardiovascular system with an implanted rotary assist device: simulation study with a refined computer model. *Artif Organs* 2002;26:349–59.
8. Lazzari CD, Darowski M, Ferrari G, Pisanelli DM, Tosti G. Modelling in the study of interaction of hemopump device and artificial ventilation. *Comput Biol Med* 2006;36:1235–51.
9. Korakianitis T, Shi Y. Numerical comparison of hemodynamics with atrium to aorta and ventricular apex to aorta vad support. *ASAIO J* 2007;53:537–48.
10. Reesink K, Dekker A, van der Nagel T, et al. Physiologic-insensitive left ventricular assist predisposes right-sided circulatory failure: a pilot simulation and validation study. *Artif Organs* 2004;28:933–9.
11. Ferreira A, Chen S, Simaan MA, Boston JR, Antaki JF. A nonlinear state-space model of a combined cardiovascular system and a rotary pump. in *Proceedings of the 44th IEEE Conference on Decision and Control, and the European Control Conference 2005*, Seville, Spain, 2005;897–902.
12. Vandenberghe S, Segers P, Meyns B, Verdonck PR. Effect of rotary blood pump failure on left ventricular energetics assessed by mathematical modeling. *Artif Organs* 2002;26:1032–9.
13. Wu Y, Allaire PE, Tao G, Olsen D. Modeling, estimation, and control of human circulatory system with a left ventricular assist device. *IEEE Trans Control Syst Technol* 2007;15:754–67.
14. Morley D, Litwak K, Ferber P, et al. Hemodynamic effects of partial ventricular support in chronic heart failure: results of simulation validated with in vivo data. *J Thorac Cardiovasc Surg* 2007;133:21–8.
15. Endo G, Araki K, Kojima K, Nakamura K, Matsuzaki Y, Onitsuka T. The index of motor current amplitude has feasibility in control for continuous flow pumps and evaluation of left ventricular function. *Artif Organs* 2001;25:697–702.
16. Lim E, Dokos S, Cloherty SL, et al. Parameter-optimized model of cardiovascular-rotary blood pump interactions. *IEEE Trans Biomed Eng* 2010;57:254–66.
17. Guyton AC, Hall JE. *Textbook of Medical Physiology*. Philadelphia, PA: W. B. Saunders Company, 1996.
18. Vandenberghe S, Nishida T, Segers P, Meyns B, Verdonck P. The impact of pump speed and inlet cannulation site on left ventricular unloading with a rotary blood pump. *Artif Organs* 2004;28:660–7.
19. Moscato F, Vollkron M, Bergmeister H, Wieselthaler G, Leonard E, Schima H. Left ventricular pressure-volume loop analysis during continuous cardiac assist in acute animal trials. *Artif Organs* 2007;31:369–76.
20. Reesink K, Dekker A, Van der Nagel T, et al. Suction due to left ventricular assist: implications for device control and management. *Artif Organs* 2007;31:542–9.
21. Hillman K, Bishop G. *Clinical Intensive Care and Acute Medicine*. Cambridge: Cambridge University Press, 2004.
22. Eckberg DL, Sleight P, Folkow B. *Human Baroreflexes in Health and Disease*. Oxford, UK: Clarendon Press, 1992.
23. Linneweber J, Nonaka K, Takano T, et al. Hemodynamic exercise response in calves with an implantable biventricular centrifugal blood pump. *Artif Organs* 2001;25:1018–21.

APPENDIX

TABLE A1. *Values of nonoptimized model parameters for healthy greyhound simulations*

Parameter	Description	Value
$P_{0,pcd}$ (mm Hg)*	Pericardial end-diastolic stiffness scaling term	0.5
λ_{pcd} (mL^{-1})	Pericardial end-diastolic stiffness coefficient	0.005
$V_{0,pcd}$ (mL)	Pericardial end-diastolic volume at zero pressure	200
$E_{es,spt}$ (mm Hg/mL)	Septal end-systolic elastance	19.5
$V_{d,spt}$	Septal end-systolic volume at zero pressure	8
$P_{0,spt}$ (mm Hg)	Septal end-diastolic stiffness scaling term	0.46
λ_{spt} (mL^{-1})	Septal end-diastolic stiffness coefficient	0.17
$V_{0,spt}$ (mL)	Septal end-diastolic volume at zero pressure	8
$E_{es,la}$ (mm Hg/mL)	LA end-systolic elastance	0.30
$V_{d,la}$ (mL)	LA end-systolic volume at zero pressure	13.08
$P_{0,la}$ (mm Hg)	LA end-diastolic stiffness scaling term	0.50
λ_{la} (mL^{-1})	LA end-diastolic stiffness coefficient	0.038
$V_{0,la}$ (mL)	LA end-diastolic volume at zero pressure	13.08
$E_{es,ra}$ (mm Hg/mL)	RA end-systolic elastance	0.30
$V_{d,ra}$ (mL)	RA end-systolic volume at zero pressure	13.08
$P_{0,ra}$ (mm Hg)	RA end-diastolic stiffness scaling term	0.50
λ_{ra} (mL^{-1})	RA end-diastolic stiffness coefficient	0.038
$V_{0,ra}$ (mL)	RA end-diastolic volume at zero pressure	13.08
R_{mt} (mm Hg.s/mL)	Mitral valve resistance	0.01
R_{tc} (mm Hg.s/mL)	Tricuspid valve resistance	0.01
R_{pv} (mm Hg.s/mL)	Pulmonary valve resistance	0.025
L_{ao} (mm Hg.s^2/mL)	Aortic inertance	0.016
L_{pa} (mm Hg.s^2/mL)	Pulmonary arterial inertance	0.016
E_{sa} (mm Hg/mL)	Systemic arterial elastance	1.00
$V_{0,sa}$ (mL)	Systemic arterial unstressed volume	157.08
$V_{0,pa}$ (mL)	Pulmonary arterial unstressed volume	52.64
$V_{0,pu}$ (mL)	Pulmonary veins unstressed volume	86.57
R_{sv} (mm Hg.s/mL)	Systemic vein resistance	0.14
R_{ra} (mm Hg.s/mL)	Vena cava resistance	0.018
R_{la} (mm Hg.s/mL)	Pulmonary vein resistance	0.009

*$P_{0,pcd}$ is set to 0.01 mm Hg in the simulations to remove the pericardium effects under open chest condition.

TABLE A2. *Values of the model parameters in a healthy circulation along with optimized values to reproduce the greyhound experimental data*

Parameter	Description	Healthy	Dog 1	Dog 2	Dog 3	Dog 4	Dog 5	Mean
L_f (mm Hg.s^2/mL)	Cannula inertance	—	0.054	0.054	0.054	0.054	0.054	0.054
$P_{pu,th}$ (mm Hg/mL)	Pulmonary pressure threshold	10.0	10.0	10.0	10.0	10.0	10.0	10.0
$V_{0,lvf}$ (mL)	LV end-diastolic volume at zero pressure	10.97	4.98	6.07	13.00	5.00 ± 0.10	1.19 ± 0.03	6.05
$P_{0,lvf}$ (mm Hg)	LV end-diastolic stiffness scaling term	0.98	4.60	2.20	3.52	1.93	0.89	2.63
λ_{lvf} (mL^{-1})	LV end-diastolic stiffness coefficient	0.028	0.020	0.023	0.023	0.021	0.030	0.023
$V_{0,rvf}$ (mL)	RV end-diastolic volume at zero pressure	26.67	24.41	36.01	31.63	32.13	5.53	25.94
$P_{0,rvf}$ (mm Hg)	RV end-diastolic stiffness scaling term	0.91	3.12	2.45	2.71	3.80	2.07	2.83
λ_{rvf} (mL^{-1})	RV end-diastolic stiffness coefficient	0.041	0.020	0.014	0.013	0.014	0.018	0.016
A_{ao} (mm Hg/mL^2)	Aortic elastance coefficient	0.0055	0.0038	0.0055	0.0047	0.0033	0.0021	0.0039
$V_{0,ao}$ (mL)	Aortic unstressed volume	54.29	28.55	54.29	62.15	60.29	26.83 ± 1.08	46.42
E_{sv} (mm Hg/mL)	Systemic vein elastance	0.020	0.021	0.034	0.021	0.025	0.025	0.025
$P_{0,vc}$ (mm Hg)	Vena cava elastance scaling term	1.17	1.52	1.65	1.64	1.36	1.38	1.51
λ_{vc} (mL^{-1})	Vena cava elastance coefficient	0.018	0.021	0.018	0.017	0.023	0.017	0.019
$V_{0,vc}$ (mL)	Vena cava unstressed volume	85.66	82.11	86.16	89.35	89.43	87.22	86.85
E_{pa} (mm Hg/mL)	Pulmonary arterial elastance	0.233	0.227	0.335	0.301	0.312	0.343 ± 0.007	0.292
E_{pu} (mm Hg/mL)	Pulmonary vein elastance	0.060	0.066	0.052	0.068	0.044	0.054	0.057
R_{av} (mm Hg.s/mL)	Aortic valve resistance	0.020	0.022	0.012	0.010	0.010	0.017	0.015
R_{ao} (mm Hg.s/mL)	Aortic resistance	0.080	0.136	0.156	0.106	0.103	0.090	0.118
$k_{R,p}$ (mm Hg.s/mL)	Positive flow cannula resistance	—	0.004	0.006	0.011	0.008	0.004	0.007
$k_{R2,p}$ (mm Hg.s$^{1.7}$/mL$^{1.7}$)	Cannula resistance flow coefficient	—	0.012	0	0	0.010 ± 0.0002	0.012	0.007
$k_{R,n}$ (mm Hg.s/mL)	Negative flow cannula resistance	—	0.02	0.02 ± 0.0008	0.02	0.02	0.02	0.02
$Q_{p,r}$ (mL/s)	Cannula resistance laminar flow threshold	—	3.00	0	0	3.00	1.00	1.40

TABLE A3. *Values of the model parameters in a healthy circulation along with optimized values (mean ± standard deviation) to reproduce the greyhound experimental data under various operating conditions*

Parameter	Description	State	Healthy	Dog 1	Dog 2	Dog 3	Dog 4	Dog 5	Mean
T^* (s)	Heart period	H1	0.8	—	0.580	0.460	0.520	0.480	0.510
		H2		0.550	0.760	0.510	0.575	0.545	0.588
		H3	—	0.515	0.840	0.510	0.575	0.545	0.597
		H4	—	0.465	0.760	0.510	0.575	0.545	0.571
		H5–H7	—	—	0.760	0.510	0.575	0.545	0.598
α_{lvf} (mm Hg^{-1})	LV end-systolic stiffness denominator term	H1	0.0034	—	0.0046	0.0075	0.0072	0.0047	0.0060
		H2	—	0.0043	0.0174	—	0.0116	0.0122	0.0114
		H3	—	0.0034	0.0220	—	0.0085	0.0067	0.0102
		H4	—	0.0116	0.0073	—	0.0065	0.0035	0.0072
		H5–H7	—	—	0.0162	0.0079	0.0043	0.0043	0.0082
β_{lvf} (mL^{-1}.mm Hg^{-1})	LV end-systolic stiffness denominator coefficient	H1	25.3E-06	—	27.7E-6	12.6E-6	39.1E-6	28.7E-5 ± 6.2E-6	9.2E-05
		H2	—	33.7E-6	14.3E-6	—	0.4E-6 ± 8.1E-9	30.5E-6	2.0E-05
		H3	—	5.1E-6	23.8E-6	—	11.2E-6	9.3E-6	1.2E-05
		H4	—	1.0E-6	20.3E-6	—	3.9E-6	12.4E-6	9.4E-06
		H5–H7	—	—	67.0E-6	8.7E-6	14.8E-6	13.6E-6	2.6E-05
$V_{d,lvf}$ (mL)	LV end-systolic volume at zero pressure	H1	21.95	—	20.00	11.20	12.78	24.24	17.06
		H2	—	14.63	17.00	—	43.10	31.96	26.67
		H3	—	13.68	11.68	—	41.67	34.39	25.36
		H4	—	14.69	30.06	—	30.29	44.12	29.79
		H5–H7	—	—	12.73	30.51	48.04	49.26	35.14
α_{rvf} (mm Hg^{-1})	RV end-systolic stiffness denominator term	H1	0.0072	—	0.0176	0.0474	0.0399	0.0098	0.0287
		H2	—	0.0079	0.0174	—	0.0264	0.0274	0.0198
		H3	—	0.0385	0.0316	—	0.0377	0.0236	0.0329
		H4	—	0.0059	0.0310	—	0.0416	0.0192	0.0244
		H5–H7	—	—	0.0275	0.0172	0.0126	0.0155	0.0182
β_{rvf} (mL^{-1}.mm Hg^{-1})	RV end-systolic stiffness denominator coefficient	H1	83.9E-6	—	170.5E-6	11.7E-6	171.4E-6	86.0E-6 ± 3.5E-6	1.1E-04
		H2	—	133.4E-6	262.5E-6	—	28.0E-6	29.2E-6	1.1E-04
		H3	—	38.1E-6	109.4E-6	—	42.0E-6	26.2E-6	5.4E-05
		H4	—	196.1E-6	88.4E-6	—	85.8E-6	14.8E-6	9.6E-05
		H5–H7	—	—	5.4E-6	40.1E-6	103.7E-6	8.1E-6	3.9E-05
$V_{d,rvf}$ (mL)	RV end-systolic volume at zero pressure	H1	29.97	—	16.31	7.38	7.63	35.88	16.80
		H2	—	28.06	21.64	—	35.00	48.78	33.37
		H3	—	18.69	23.68	—	24.27	51.69	29.58
		H4	—	17.88	31.47	—	14.48	46.60	27.61
		H5–H7	—	—	37.74	41.06	49.49	64.77	48.27
R_{sa} (mm Hg.s/mL)	Systemic peripheral resistance	H1	1.43	—	1.63	0.66	0.66	0.43	0.85
		H2	—	0.32	0.89	—	0.47	1.44	0.78
		H3	—	0.39	1.38	—	0.64	1.62	1.01
		H4	—	0.64	2.84	—	1.03	1.90	1.60
		H5–H7	—	—	1.37	2.75	0.70	1.35	1.68
			—	—		2.25 (H6)			
A_{pa} (mm Hg.s/mL)	Pulmonary peripheral resistance	H1	0.18	—	0.15	0.12	0.10	0.08	0.11
		H2	—	0.09	0.12	—	0.09 ± 0.002	0.08	0.10
		H3	—	0.09	0.12	—	0.09	0.08	0.10
		H4	—	0.09	0.14 ± 0.004	—	0.09	0.08	0.10
		H5–H7	—	—	0.12	0.26	0.09	0.08	0.14
B_{pa} (mm Hg.s/mL)	Pulmonary peripheral resistance scaling term	H1	0.47	—	0.49	0.41	0.24	0.36	0.38
		H2	—	0.38	0.37	—	0.22	0.34	0.33
		H3	—	0.34	0.35	—	0.22	0.33	0.31
		H4	—	0.35	0.36	—	0.22	0.37	0.33
		H5–H7	—	—	0.32	0.07	0.22	0.38	0.25
C_{pa} (mm Hg^{-1})	Pulmonary peripheral resistance coefficient	H1	0.42	—	0.41 ± 0.009	0.40	0.28	0.33	0.36
		H2	—	0.35	0.35	—	0.26	0.36	0.33
		H3	—	0.36	0.41 ± 0.008	—	0.26 ± 0.005	0.32	0.34
		H4	—	0.38	0.39	—	0.26	0.39	0.36
		H5–H7	—	—	0.30	0.36	0.26 ± 0.005	0.37	0.32
$V_{0,sv}$ (mL)	Systemic vein unstressed volume	H1	1292.1	—	2017.2	1509.5	1969.6	1108.1	1651.1
		H2	—	1517.1	1922.1	—	1569.8	1008.3	1504.4
		H3	—	1319.1	1837.2	—	1581.2	824.9	1390.6
		H4	—	1301.1	2028.4	—	1433.3	694.3	1364.3
		H5–H7	—	—	2006.1	2094.0	2006.3	1148.2	1813.7
V_{total} (mL)	Total blood volume	H1–H4 & H6	3400.0	3400.0	3400.0	3400.0	3400.0	3400.0	3400.0
		H5	—	—	2954.0	3150.0	2864.0	2850.0	2954.5
		H7	—	—	3831.0	3839.0	3952.0	3940.0	3890.5
$E_{es,lvf}$** (mm Hg/mL)	LV end-systolic elastance	H1	4.59	—	3.81	4.77	6.00	3.30	4.47
		H2	—	2.98	1.36	—	0.86	1.11	1.58
		H3	—	6.56	1.76	—	1.14	1.70	2.79
		H4	—	10.88	1.51	—	2.18	2.01	4.15
		H5–H7	—	—	1.98	1.59	1.76	1.71	1.76

E. LIM ET AL.

TABLE A3. *Continued*

Parameter	Description	State	Healthy	Dog 1	Dog 2	Dog 3	Dog 4	Dog 5	Mean
$V_{d,lvf,lin}$** (mL)	LV end-systolic	$H1$	10.97	—	5.00	4.20	9.59	4.20	5.75
	volume at	$H2$–$H4$	—	9.77	6.45	17.04	25.5	14.26	14.60
	zero pressure	$H5$–$H7$	—	—	15.33	17.04	35.0	14.26	20.41
$E_{es,rvf}$**	RV end-systolic	$H1$	1.99	—	1.29	1.60	1.70	1.10	1.42
(mm Hg/mL)	elastance	$H2$	—	0.66	0.72	—	0.35	0.33	0.52
		$H3$	—	2.60	0.49	—	0.65	0.35	1.02
		$H4$	—	3.65	0.36	—	1.18	0.52	1.43
		$H5$–$H7$	—	—	0.40	0.71	0.57	0.39	0.52
$V_{d,rvf,lin}$** (mL)	RV end-systolic	$H1$	26.68	—	9.62	6.02	6.00	−6.50	3.79
	volume at	$H2$–$H4$	—	13.48	9.62	—	29.0	28.60	20.18
	zero pressure	$H5$–$H7$	—	—	15.62	33.57	40.00	28.60	29.45

Mean values of the optimized parameters over all the five animals were listed in the last column. In the dog 1 experiment, a beta-blocker was not used and preload dependence tests were not carried out; therefore $H2$–$H4$ in dog 1 corresponded to the afterload dependence test under healthy heart conditions. In the dog 3 experiment, it was observed that vena cava pressure (P_{vc}) continuously declined during the afterload dependence test, most probably due to loss in total blood volume; therefore the $H2$–$H4$ data was discarded.

*These values were either estimated or determined directly from the greyhound experimental measurements, and not via least squares optimization.

**Parameter values of the linearized ESPVR.